Published online 29 November 2008

Nucleic Acids Research, 2009, Vol. 37, No. 2 ***e10***
doi:10.1093/nar/gkn965

Molecule-level imaging of Pax6 mRNA distribution in mouse embryonic neocortex by molecular interaction force microscopy

Yu Jin Jung[1], Yu Shin Park[2], Ki-Jun Yoon[3], Young-Yun Kong[3], Joon Won Park[1,*] and Hong Gil Nam[2,3,4,*]

[1]Center for Integrated Molecular Systems, Department of Chemistry, [2]National Core Research Center for Systems Bio-Dynamics, [3]Division of Molecular and Life Sciences and [4]School of Interdisciplinary Bioscience and Bioengineering, Pohang University of Science and Technology, San 31 Hyoja-dong, Pohang, 790-784, South Korea

Received August 12, 2008; Revised November 14, 2008; Accepted November 16, 2008

ABSTRACT

Detection of the cellular and tissue distributions of RNA species is critical in our understanding of the regulatory mechanisms underlying cellular and tissue differentiation. Here, we show that an atomic force microscope tip modified with 27-acid dendron, a cone shaped molecule with 27 monomeric units forming its base, can be successfully used to map the spatial distribution of mouse Pax6 mRNA on sectioned tissues of the mouse embryonic neocortex. Scanning of the sectioned tissue with a 30-mer DNA probe attached to the apex of the dendron resulted in detection of the target mRNA on the tissue section, permitting mapping of the mRNA distribution at nanometer resolution. The unprecedented sensitivity and resolution of this process should be applicable to identification of molecular level distribution of various RNAs in a cell.

INTRODUCTION

Differential expression of mRNA in various cell types is a basic regulatory mechanism of cellular and/or tissue differentiation (1,2). Intracellular RNA distribution is now recognized as an essential mechanism in the regulation of localized protein expression. Yet, the sensitivity and resolution of current technologies are not sufficient for understanding the molecular level roles of mRNA concentration and distribution. Atomic force microscopy (AFM) (3,4) permits recognition of proteins by utilizing antigen–antibody (5–7) or ligand–receptor interactions (8–11), which subsequently allow spatial distribution mapping at nanometer resolution. Here, we demonstrate the feasibility of mapping mRNA distribution in a biological tissue sample by measuring DNA–RNA interaction forces with AFM. As a model system, we chose mouse Pax6 expressed in the embryonic neocortex (12–16). The mouse *Pax6* gene encodes a transcription factor that plays a pivotal role in the development of embryonic neuronal cells (13,15,17) and of a few other organs, including the eye (18). In the embryonic neocortex of mouse, Pax6 is preferentially expressed in radial glial cells, which are progenitors of neuronal and glial cells (14,19). The somas of radial glial cells are mostly located in the ventricular and subventricular zones of the neocortex where Pax6 mRNA is abundant.

When measuring molecular interactions with AFM (10–11,20–22), the way of immobilizing a probe molecule on the AFM tip is critical. Less-controlled immobilization, in terms of specificity, orientation, and spacing, can result in poor detection of target molecules, leading to unwanted nonspecific interactions and/or broad unbinding force distributions (23–25). We previously demonstrated that immobilization of a DNA probe on a dendron-modified AFM tip simplifies the force–distance curves for the DNA–DNA interaction, thereby enhancing the reliability of the analysis (26). Dendron is a conically shaped molecule where the repeating monomeric units are directionally stretched from a core monomer at the apex side (27–29) (Figure 1A and Supplementary Figure S2A). Thus, modification of the AFM tip surface with dendrons and subsequent attachment of a probe molecule on the apex of the

*To whom correspondence should be addressed. Tel: +82 54 279 2119; Fax: +82 54 279 0653; Email: jwpark@postech.ac.kr
Correspondence may also be addressed to Hong Gil Nam. Tel: +82 54 279 2111; Fax: +82 54 279 5972; Email: nam@postech.ac.kr
Present Address:
Yu Jin Jung, Biotechnology Center, University of Technology Dresden, 01307 Dresden, Germany

The authors wish it to be known that, in their opinion, the first two authors should be regarded as joint First Authors.

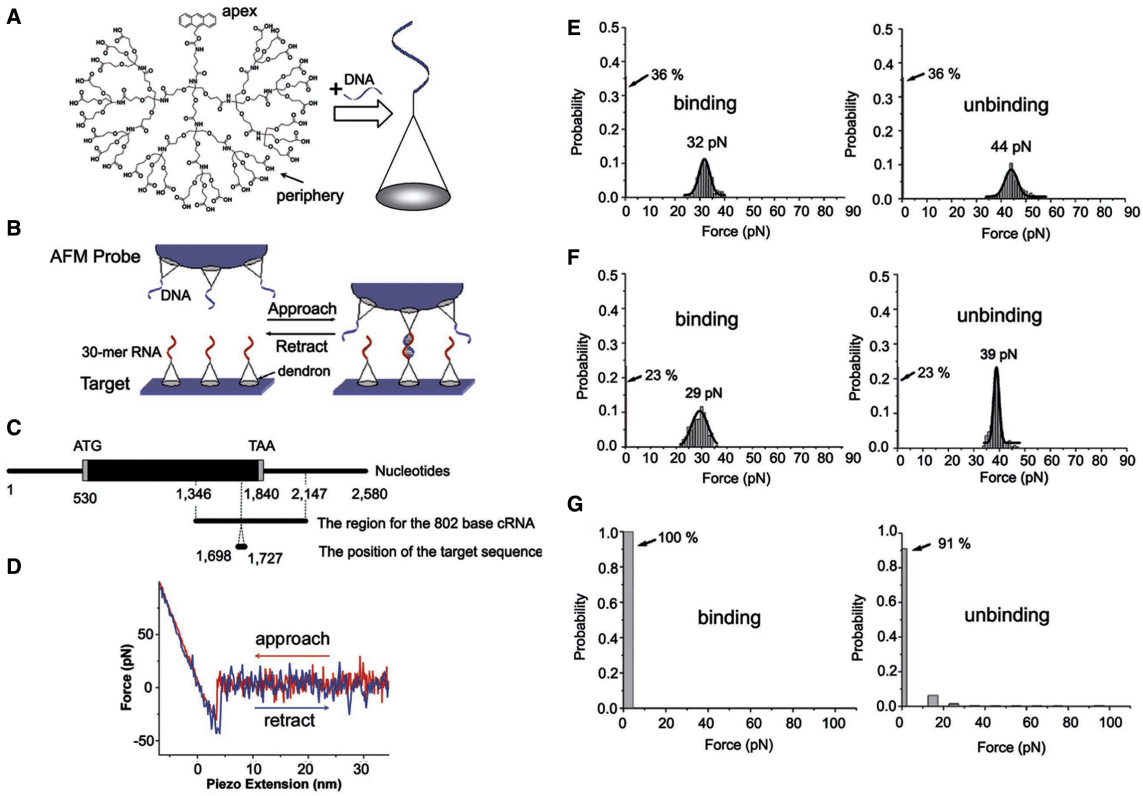

Figure 1. Measurement of the binding and unbinding forces between the 30-mer DNA probe on the AFM tip and the complementary oligo RNA on the silicon surface. (**A**) Structure of the 27-acid dendron, 9-anthrylmethyl-3-({[*tris*({[(1-{*tris*[(2-{[(*tris*{[2-carboxyethoxy]methyl}methyl)amino]carbonyl}ethoxy)methyl]methyl}amino)carbonyl]-2-ethoxy}methyl)methyl]amino}carbonyl)propylcarbamate. Shown to the right is a schematic diagram of the DNA probe attached to the apex of a dendron on a substrate such as an AFM tip. (**B**) A schematic drawing of the experimental setup employed for the measurement of the interaction force between the 30-mer DNA probe and the complementary 30-mer oligo RNA. The DNA probe complementary to the sequence between nucleotides 1698–1727 of the Pax6 mRNA was immobilized on the 27-acid dendron–modified AFM tip. The 30-mer oligo RNA complementary to the DNA probe sequence was immobilized on a 27-acid dendron-modified silicon substrate. (**C**) Structure of Pax6 mRNA. The DNA sequence complementary to the mRNA sequence between nucleotides 1698–1727 was used in the synthesis of the DNA probe, 5′-$NH_2(CH_2)_6$-TGG GCT GAC TGT TCA TGT GTG TTT GCA TGT-3′. (**D**) A typical force–distance curve for the interaction between the DNA probe and the 30-mer oligo RNA. Forces were recorded at a measurement rate of 0.54 μm s^{-1}. (**E**) The histograms of the binding (left) and unbinding (right) forces derived from the force–distance curves of the interaction between the DNA probe and the complementary 30-mer RNA. In this example, the histogram was obtained from 191 cycles of approach and retraction. The frequency of detection for the binding and unbinding events during this process was 64%. Gaussian fitting gave the most probable force values of 32 and 44 pN for the binding and unbinding events, respectively. (**F**) The histograms of the binding (left) and unbinding (right) forces between the DNA probe on the 9-acid dendron-modified tip and the complementary 30-mer DNA oligonucleotides on the 9-acid dendron-modified silicon substrate. The histogram was obtained from 275 cycles of approach and retraction. The frequency of detection for the binding and unbinding events during this process was 77%. Gaussian fitting gave a mean force value of 29 and 39 pN for binding and unbinding events, respectively. (**G**) The histograms of binding (left) and unbinding (right) forces between the DNA probe and a non-complementary 30-mer oligo RNA. The sequence of the non-complementary RNA is 5′-$NH_2(CH_2)_6$-UGG GCU GAC UGU UCA UGU GUG UUU GCA UGU-3′. The histogram was obtained from 515 cycles of approach and retraction.

dendron allows controlled spacing between the probe molecules (Figure 1A and Supplementary Figure S1). Here, we utilized a DNA probe attached to a dendron-modified AFM tip to measure the specific adhesive force to the complementary RNA and Pax6 mRNA of 802 bases, and to map the Pax6 mRNA distribution on the surface of sectioned mouse embryonic tissues.

MATERIALS AND METHODS

General

A silane coupling agent *N*-[3-(triethoxysilyl)propyl]-*O*-polyethyleneoxide urethane (TPU) was purchased from Gelest. All other chemicals are of reagent grade from Sigma-Aldrich. UV-grade fused silica plates were purchased from CVI Laser. Polished Si(100) wafers (dopant: phosphorus; resistivity: 1.5–2.1 Ω cm) were purchased from MEMC Electronic Materials. Deionized water (18 MΩ cm) was obtained by passing distilled water through a Barnstead E-pure 3-Module system. All water used in RNA experiments was pretreated overnight with diethylpyrocarbonate (DEPC, 0.05% v/v) and subsequently autoclaved. All short oligonucleotides were purchased from Samchully Pharm (Korea).

Sample preparation

Cleaning the substrates. Silicon wafers and fused silica plates (for dendron surface coverage analysis; data not

shown) were sonicated in Piranha solution [concentrated H_2SO_4:30% H_2O_2 = 7:3 (v/v) for 4 h]. The substrates were then washed thoroughly with deionized water and subsequently immersed in a mixture of deionized water, concentrated ammonia solution, and 30% hydrogen peroxide [5:1:1 (v/v/v)] in a Teflon beaker. The beaker was placed in a water bath and heated at 80°C for 10 min. The substrates were taken out of the solution and rinsed thoroughly with deionized water. The substrates were again placed in a Teflon beaker containing a mixture of deionized water, concentrated HCl, and 30% H_2O_2 [6:1:1 (v/v/v)]. The beaker was heated at 80°C for 10 min. The substrates were taken out of the solution and washed thoroughly with copious deionized water. The clean substrates were dried in a vacuum chamber (30–40 mTorr) for about 30 min and used immediately for the next steps.

AFM probe pretreatment. Standard V-shaped silicon nitride cantilevers with pyramidal tips (MLCT-AUNM, Veeco Instruments; k = 10 pN/nm) were first oxidized by dipping in 80% nitric acid and then heated at 80°C for 20 min. The cantilevers were removed from solution and washed thoroughly with copious deionized water. The clean cantilevers were dried in a vacuum chamber (30–40 mTorr) for about 30 min and used immediately for the next steps.

Silylation. Silicon/silica substrates and cantilevers were immersed in anhydrous toluene (20 ml) containing the silane coupling agent (0.20 ml) under a nitrogen atmosphere for 4 h. After silylation, the substrates and cantilevers were washed with toluene, and then baked for 30 min at 110°C. The substrates were immersed in toluene, toluene–methanol [1:1 (v/v)], and methanol in a sequential manner and sonicated for 3 min in each washing solution. The cantilevers were rinsed thoroughly with toluene and methanol in a sequential manner. Finally, the substrates and cantilevers were dried under vacuum (30–40 mTorr).

Preparation of dendron modified surfaces

Preparation of 9-acid dendron modified surfaces. The hydroxylated substrates and cantilevers were immersed for 12–24 h in a methylene chloride solution dissolving the 9-acid dendron (1.0 mM), a coupling agent, 1,3-dicyclohexylcarbodiimide (DCC) (9.9 mM), and 4-dimethylaminopyridine (DMAP) (0.9 mM). The 9-acid dendron, 9-anthrylmethyl *N*-({[*tris*({2-[({*tris*[(2-carboxyethoxy) methyl]methyl}amino)carbonyl]ethoxy}methyl)methyl] amino}carbonyl)propylcarbamate (or 9-acid, see Supplementary Figure S2A) used in this work was prepared by us, and dissolved in a minimum amount of dimethylformamide (DMF) prior to adding into methylene chloride. After the reaction, the substrates were immersed in methylene chloride, methanol, and water in a sequential manner, and were sonicated for 3 min at each washing step. The cantilevers were rinsed thoroughly with methylene chloride, methanol and water in a sequential manner. Finally the substrates and cantilevers were washed with methanol, and dried under vacuum (30–40 mTorr).

Preparation of 27-acid dendron modified surfaces. The above hydroxylated substrates and cantilevers were immersed for 12–24 h in a methylene chloride solution dissolving the 27-acid dendron (1.0 mM), a coupling agent, 1,3-dicyclohexylcarbodiimide (DCC) (29.7 mM), and 4-dimethylaminopyridine (DMAP) (2.9 mM). The 27-acid dendron, 9-anthrylmethyl-3-({[*tris*({[(1-{*tris*[(2-{[(*tris*{[2-carboxyethoxy]methyl}methyl)amino]carbonyl} ethoxy)methyl]methyl}amino)carbonyl]-2-ethoxy}methyl) methyl]amino}carbonyl)propylcarbamate (or 27-acid, see Figure 1A) used in this work was prepared by us (see Supplementary Data), and dissolved in a minimum amount of DMF prior to adding into methylene chloride. After the reaction, the substrates were immersed in methylene chloride, methanol, and water in a sequential manner, and were sonicated for 3 min at each washing step. The cantilevers were rinsed thoroughly with methylene chloride, methanol and water in a sequential manner. Finally the substrates and cantilevers were washed with methanol, and dried under vacuum (30–40 mTorr).

Deprotection of the 9-anthrylmethoxycarbonyl group

The cantilevers and dendron-modified substrates were stirred for 2 h in a methylene chloride solution containing trifluoroacetic acid (TFA) (1.0 M). After the reaction, they were soaked in a methylene chloride solution with 20% (v/v) diisopropylethylamine (DIPEA) for 10 min. The substrates were sonicated in methylene chloride and methanol each for 3 min, and the cantilevers were rinsed thoroughly with methylene chloride and methanol in a sequential manner. The substrates and cantilevers were dried under vacuum (30–40 mTorr).

Preparing NHS-modified substrates

The above deprotected substrates and cantilevers were immersed for 4 h under nitrogen in an acetonitrile solution containing di(N-succinimidyl)carbonate (DSC) (25 mM) and DIPEA (1.0 mM). After the reaction, the substrates and cantilevers were placed in stirred DMF for 30 min and washed with methanol. The substrates and cantilevers were dried under vacuum (30–40 mTorr).

Immobilization of DNA/isolated short RNA

The above NHS-modified substrates were placed in a solution containing 30-mer RNA [20 μM in 25 mM $NaHCO_3$ buffer (pH 8.5) with 5.0 mM $MgCl_2$] for 12 h. In parallel, the NHS-modified cantilevers were placed in a solution of 30-mer DNA [20 μM in 25 mM $NaHCO_3$ buffer (pH 8.5) with 5.0 mM $MgCl_2$] for 12 h. The sequence of the 30-mer RNA is 5′-$NH_2(CH_2)_6$-ACA UGC AAA CAC ACA UGA ACA GUC AGC CCA-3′, and its complementary 30-mer DNA sequence is 5′-$NH_2(CH_2)_6$-TGG GCT GAC TGT TCA TGT GTG TTT GCA TGT-3′, of which GC content is 47%. After the reaction, the substrates and cantilevers were stirred in a buffer solution [2× SSPE buffer (pH 7.4) containing 7.0 mM sodium dodecylsulfate] at 37°C for 1 h, and were rinsed thoroughly with water to remove non-specifically bound oligonucleotides.

Finally, the substrates and cantilevers were dried under vacuum (30–40 mTorr).

Preparation of mouse embryonic tissue sections

Brains from C57BL/6 mouse embryos at E14.0 were dissected in PBS buffer and fixed with gentle rocking for 12 h in 4% paraformaldehyde (PFA) at 4°C. Plug date was defined as embryonic day 0.5 (E0.5). The brain tissue was then washed in PBS buffer with 4% PFA and rinsed briefly in an embedding medium (Tissue-Tec, USA). The brain tissues in the embedding medium were fast-frozen in isopentane cooled with liquid nitrogen. Serial coronal sections of 12 μm thickness were prepared with a freezing microtome and were collected on glass slides (ProbeOn plus, Fisher Scientific, USA). Tissue sections were fixed with 4% PFA in PBS buffer for 10 min and rinsed with PBS solution before treatment with Proteinase K (4 μg/ml) in PBS buffer for 8 min at room temperature. Tissue sections were post-fixed with 4% PFA, rinsed with PBS, dehydrated sequentially in 70% and 95% ethanol for a few seconds before air-drying. The *in situ* hybridization of the embryonic tissue sections was basically performed according to a standard protocol (30).

AFM force measurements

All force measurements were performed with a NanoWizard AFM (JPK Instrument). The spring constant of each AFM tip was calibrated in solution before each experiment by the thermal fluctuation method. The spring constants of the cantilevers employed varied between 10 and 15 pN/nm. All measurements were carried out in fresh PBS buffer (pH 7.4) at room temperature. All force measurements were recorded with a measurement velocity of 0.54 $\mu m\,s^{-1}$.

Force measurements of model systems. To measure the mean force values, the force–distance curves were always recorded more than 100 times at one position on a substrate, and more than two spots were examined in each separate experiment.

Force measurements for tissues. Force images were obtained by processing the force values recorded during the raster-scanning on areas of 300 nm × 300 nm each. The area was divided by 10 × 10 pixels. Concerning statistics and stochastic behaviour, force–distance curves were typically recorded more than 10 times at each pixel, and the presented force value of each pixel is the mean unbinding force from fitting the force distribution to a Gaussian curve.

RESULTS

The interaction force between DNA and 30-mer RNA (Model system I)

We first measured the interaction force between the DNA probe immobilized on the AFM tip and the 30-mer oligo RNA complementary to the DNA probe on the silicon wafer (Figure 1B). To immobilize DNA probe and 30-mer oligo RNA on the AFM tip and silicon wafer, we initially employed the so-called 9-acid dendron. The 9-acid dendron led to satisfactory measurement of DNA–DNA interaction forces in our previous study (26); conjugation between the nine carboxylic acids in the periphery of the dendron (Supplementary Figure S2A) and the AFM tip surface provided mesospacing for the DNA probes attached to the apex. While the DNA probe on the 9-acid dendron-modified AFM tip properly detected the complementary target oligo RNA molecule, it yielded an unsatisfactorily broad force distribution histogram for a longer target RNA (Supplementary Figure S2B). Employment of a 27-acid dendron (Figure 1A) that provided larger spacing between the DNA probes on the apex yielded an interaction force histogram satisfactorily narrow for analysis of the DNA–RNA interactions (see below). Here, we describe our analysis of the interaction force mapping of mRNA with the 27-acid dendron-modified AFM tip.

The DNA probe used was a 30-mer oligonucleotide complementary to nucleotides 1698–1727 of Pax6 mRNA (Figure 1C and Supplementary Figure S3). The DNA probe with an amine group at the 5′ side was covalently linked to the apex of a 27-acid dendron immobilized on the AFM tip. The target RNA with an amine group at the 5′ position was attached to the apex of an immobilized 27-acid dendron on the surface of a silicon wafer. We obtained force–distance curves of the interaction between the DNA probe and target RNA during the approach and retraction processes, respectively. The measurement was repeated more than 100 times for each spot, with measurement rates of 0.54 $\mu m\,s^{-1}$. The resulting force–distance curves showed a single distinctive binding (attractive) and unbinding (adhesive) pattern during the approach and retraction processes, respectively (Figure 1D). Binding and unbinding forces were obtained from each force–distance curve to generate force histograms (Figure 1E). Gaussian fitting of these histograms yielded mean forces of 32 and 44 pN for the binding and unbinding events, respectively. In this experiment, the binding and unbinding forces were same as those measured with the 9-acid dendron–modified AFM tip (data not shown).

It is known that an RNA–DNA duplex is more stable than the corresponding DNA–DNA interaction (31). The corresponding DNA–DNA interaction was measured with the 9-acid dendron–modified AFM tip and silicon substrate and at a 0.54 $\mu m\,s^{-1}$ measurement rate (Figure 1F). In order to avoid the error that might occur during the calibration process, we employed an identical tip for the comparison in this particular experiment. It was possible to use one tip for both experiments because the only thing we had to change was the substrate. The interaction binding and unbinding forces were smaller than those of the DNA–RNA interaction by 3 and 5 pN, respectively. To verify the specificity, interactions between the probe DNA and non-complementary target RNA were measured. Binding was not observed, the unbinding force was significantly less than the specific mean force, and the unbinding frequency was dramatically reduced (Figure 1G).

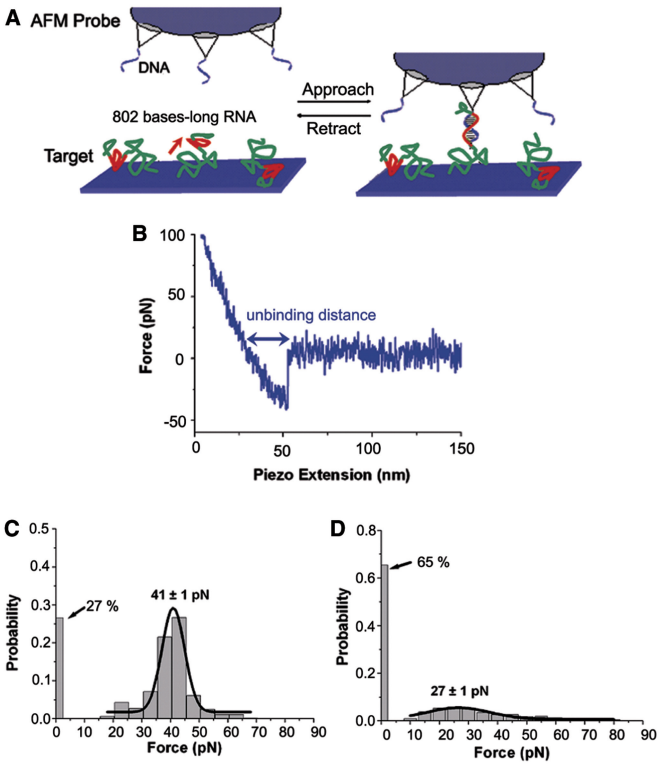

Figure 2. Measurement of the unbinding forces between the 30-mer DNA probe on the AFM tip and the 802-base cRNA immobilized on a glass slide. (**A**) A schematic drawing of the experimental setup. The 802-base cRNA of the Pax6 mRNA containing the sequence complementary to the DNA probe sequence (red color, arrow) was immobilized on a glass slide. (**B**) A typical force–distance curve for the interaction between the DNA probe and cRNA. Forces were recorded at a measurement rate of 0.54 μm s^{-1}. (**C**) The histogram of unbinding forces derived from the force–distance curves of the interaction between the DNA probe and the cRNA. The histogram was obtained from 870 cycles of approach and retraction. The frequency of detection for unbinding events during the retraction process was 73% in this example. The Gaussian fitting gave the mean value of 41 ± 1 pN. The statistical error was estimated by $2\sigma/\sqrt{N}$, where σ is the width of the distribution of the N rupture events in the histogram. (**D**) The histograms of the unbinding forces between the DNA probe and antisense cRNA. The 802-base antisense RNA of Pax6 mRNA was synthesized *in vitro* and immobilized on a glass slide. The histogram was obtained from 657 cycles of approach and retraction.

The interaction forces between DNA and partial-length Pax6 RNA of 802 bases (Model system II)

We next examined the interaction force between the AFM tip-bound DNA probe and its complementary RNA sequence residing in a long RNA molecule (Figure 2A). The 802-base RNA (cRNA) corresponding to nucleotides 1346–2147 of Pax6 mRNA (Figure 1C) was synthesized *in vitro* (see Supplementary Data). This cRNA, which included nucleotides 1698–1727 complementary to the probe DNA sequence, was fixed on a glass slide (see Supplementary Data). Binding and unbinding force curves between the 30-mer DNA probe on the dendron-modified tip and cRNA on the slide were obtained as above. Force–distance curve patterns during the retraction process indicated mostly single (Figure 2B and Supplementary Figure S4) and double (Supplementary Figure S5A) unbinding events with a rarity of more than two unbinding events (Supplementary Figure S5B). The multiple unbinding events might be explained by poor control of the surface density of 802-base cRNA and secondary interactions with neighboring cRNA.

The unbinding forces for multiple unbinding events calculated from the last rupture event were incorporated into the force histogram. These mean unbinding forces between the DNA probe and the cRNA from each spot ranged from 39 to 41 pN (Figure 2C and Supplementary Figure S6). The unbinding probability from each spot is different each other because the surface fixation method results in randomly oriented 802-base RNA on surface. The orientation of 802-base RNA on the glass slide should give minimal influence on the mean unbinding force. The only thing that would change is the probability of recording the interaction. The observed forces were from specific interactions between the DNA probe and cRNA sequence, since the force histogram for interactions with the antisense sequence cRNA was quite different, with a reduced mean unbinding force (27 pN) and frequency of unbinding events (Figure 2D). The mean unbinding force of the 802-base cRNA (39–41 pN) was slightly less than that of the 30-mer oligo RNA (44 pN).

Mapping of Pax6 mRNA on a mouse embryonic tissue

We mapped the distribution in mouse E14.0 embryonic brain tissue, when Pax6 mRNA is expressed in the ventricular and subventricular zones (13–15). The brain tissue was sectioned and fixed to expose mRNA on its surface (see Supplementary Data). We confirmed Pax6 mRNA expression in the neocortical region by *in situ* hybridization with a digoxigenin-labeled antisense Pax6 RNA probe (see Supplementary Data). Consistent with previous reports (13–15), Pax6 mRNA was much more abundant along the ventricular zone than along the cortical plate side (Figure 3A). The ventricular zone and cortical plate sides were then subjected to mRNA mapping, employing the same conditions used nucleotides for detection of cRNA immobilized on glass. Pax6 mRNA mapping was performed by detecting the specific unbinding force between the DNA probe and Pax6 mRNA on the sectioned tissue (Figure 3B). In each mapping area, 10 × 10 pixels were examined to obtain force–distance curves for the unbinding processes. Representative force distance curves for single rupture unbinding events are shown in Supplementary Figure S7. The mean unbinding force value for each pixel was determined from the histograms of the unbinding forces (Supplementary Figure S8) recorded more than 10 times. The mean unbinding force of each pixel was displayed as a force map by categorizing the force values into eight levels (Figure 3B), with a reference point at 37 pN, as the mean unbinding force distribution of each pixel showed a distinctive trough between 33 and 36 pN (Supplementary Figure S9A). Of the 600 pixels examined, no single pixel showed the value in this range. We considered any force over 37 pN to be derived from the specific interaction between the DNA probe and Pax6 mRNA, while the reason for the deviation from

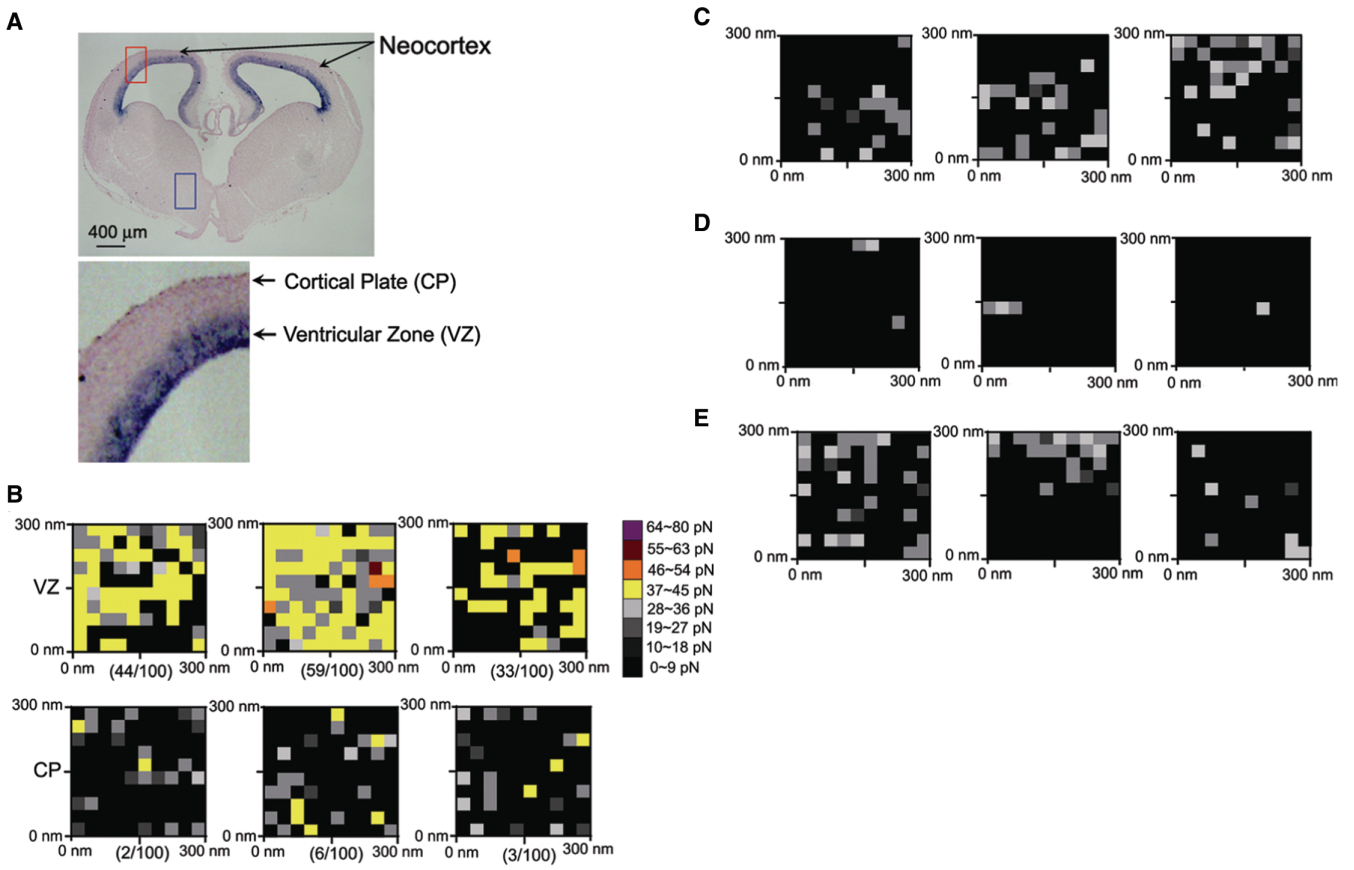

Figure 3. Mapping distribution of the Pax6 mRNA in sections of mouse embryonic tissue. (**A**) Expression of the Pax6 mRNA in a coronal section of a mouse embryonic brain examined by *in situ* hybridization. The mRNA was detected with a digoxigenin-11-UTP-labeled anti-sense Pax6 RNA probe. Blue staining represents the presence of the labeled probe and thus expression of the Pax6 mRNA, which was detected by alkaline phosphatase-coupled anti-digoxigenin antibody. The neocortex part of the coronal section noted by a red box (upper) is enlarged in the lower panel. Note that Pax6 mRNA was most abundant in the ventricular zone. A part of striatum where Pax6 mRNA is not expressed is marked by a blue box and used as a negative control area in (E) below. (**B**) Maps of Pax6 mRNA distribution. Three 300 nm × 300 nm areas in each of the ventricular (upper) and cortical plate (lower) zones were scanned. Each of the 300 nm × 300 nm area was divided into 10 × 10 pixels for detection of the interaction force. The interaction forces were categorized into eight levels and noted by variable colors. The number in the parenthesis indicates the number of pixels that have a mean adhesive force greater than 36 pN. (**C**) The force maps after blocking the DNA probe-binding site in mRNA with a free competitive 30-mer DNA. The DNA sequence, 5′-TGG GCT GAC TGT TCA TGT GTG TTT GCA TGT-3′, which is the same as that of the probe DNA on the AFM tip, was incubated with the tissue section at a concentration of 40 μM for 40 min prior to measurement of force–distance curves. (**D**) The force maps after treatment of the tissue section with RNase. The force–distance curves were recorded after incubating the tissue sample with RNase A (20 μg/ml) at 37°C for 30 min. (**E**) The force maps of Pax6 mRNA distribution in the striatum region of the coronal section. Note that no interaction force was larger than 33 pN.

41 pN observed in 802-base RNA was not clear, complication in tissue sample should be one of the reasons for this deviation. As the controls, no force over 33 pN was observed in tissues blocked by oligo DNA complementary to the mRNA (Figure 3C), in RNAse-treated tissues (Figure 3D), or in the control area of the tissue sections (Figure 3E). The largest forces observed in these cases were 33, 31 and 33 pN (Supplementary Figure S9B), respectively.

DISCUSSION

In case of an 802-base cRNA and a fixed mouse embryonic brain tissue, interestingly, no distinctive binding events were recorded in the force–distance curve of the interaction between the DNA probe and cRNA. The absence of the binding event could be explained by the fact that the DNA binding site is located at the inner part of 802-base-long cRNA and Pax6 mRNA with which exists in the form of complicated secondary structures (Figure 2A). In addition, force curves demonstrated nonlinear unbinding profiles prior to unbinding rupture (Figure 2B and Supplementary Figures S4, S5A and S5B), whereas those of the 30-mer RNA manifested linear profiles (Figure 1D). This difference was likely due to the enhanced flexibility of the 802-base cRNA and Pax6 mRNA, which should result in a reduced actual loading rate during unbinding (22). In particular, the unbinding distance in the force curves of 802-base cRNA and Pax6 mRNA, varied in the range of 8–40 nm, while that of the 30-mer oligo RNA varied in the range of 3–7 nm. The rupture distance of 802-base cRNA and Pax6 mRNA reflect the rupture distance of 30-mer RNA and

the forced extension of a certain parts of 802-base cRNA fixed on the solid surface and Pax6 RNA embedded in the tissue. Force–distance curve patterns during the retraction process of 802-base cRNA indicated mostly single (Figure 2B and Supplementary Figure S4) and double (Supplementary Figure S5A) unbinding events with a rarity of more than two unbinding events (Supplementary Figure S5B). The multiple unbinding events might be explained by poor control of the surface density of 802-base cRNA and secondary interactions with neighboring cRNA. Notably, the tissue sample demonstrated more frequent multiple unbinding events than the cRNA samples (Supplementary Figure S5C and D). Other neighboring mRNAs of which sequences are partially identical to that of the targeted RNA might cause the multiple rupture events.

Force maps indicated that Pax6 mRNA is was detected at a much higher frequency in the ventricular zone than in the cortical plate zone. In the force map in Figure 3B, the numbers of the positive pixels were 136 and 11 for the ventricular and cortical plate zones, respectively, out of 300 pixels examined. Thus, the frequency of positive pixels in the two zones was proportional to Pax6 mRNA levels detected by *in situ* hybridization, supporting the concept that these force maps reflect the local distribution of Pax6 mRNA in a given area of tissue. From several control experiments including the force maps in the control area of the tissue sections of Figure 3A, presence of Pax6 mRNA in cortical plate was clearly confirmed. Because the probe DNA detects only the mRNA molecules appeared on the surface of the examined tissue that are accessible to the probe, it is difficult to suggest that the number of the pixels with a certain force value is linearly dependent to the mRNA on surface of the examined tissue. Also, the hydrodynamic length of the probe DNA would allow sensing mRNA at the neighboring pixel. Nevertheless, it is expected that most of mRNA molecules present at the tissue surface were sensed because the orientation of mRNA at the surface would affect minimally the most probable adhesive force, while the probability of recording an interaction would be influenced. Therefore, it is believed that the force maps recorded by picoforce AFM correctly shows the trend of the mRNA distribution. It is important to note the high sensitivity of the employed approach enables the detection of the mRNA in the ventricular zone, while the Pax6 protein has not been detected by the fluorescence assay in the section.

CONCLUSIONS

In conclusion, the presence and location of mRNA molecules in a sectioned tissue can be facilely detected using a DNA probe attached to a dendron-modified AFM tip. This mRNA detection procedure is straightforward once the DNA probe is properly selected and immobilized on a suitably modified AFM tip. The choice of dendron in AFM tip modification was a critical factor. The use of a 27-acid dendron led to successful detection of the mRNA, whereas tips modified with a lower generation dendron (3-acid or 9-acid) led to unsatisfactory results, with frequent nonspecific and multiple rupture events and broad force histograms (Supplementary Figures S10 and S11). The use of AFM to detect mRNA via molecular interaction force provides a molecular level of sensitivity. In contrast, the sensitivity of *in situ* hybridization is limited even with fluorescent probes. In this regard, it is notable that the force map we obtained indicates the clear presence of mRNA in the cortical plate area, whereas *in situ* hybridization was not sufficient to distinguish the low level expression of mRNA in this area (12,13) (Figure 3A). AFM provided nano- or molecular-level resolution for the distribution of mRNA in a tissue (Figure 3B), although the hydrodynamic length of the probe DNA and target RNA may limit this resolution. The unprecedented sensitivity and resolution in mapping mRNA with this approach should open doors to unexplored biological areas. The presence and localization of various RNA species may be detected with single-molecule sensitivity and resolution. Diagnostic examination for the presence of a specific mRNA species should also be feasible directly from tissue samples.

SUPPLEMENTARY DATA

Supplementary Data are available at NAR Online.

ACKNOWLEDGEMENTS

J.W.P. acknowledges valuable comments from Professors Saul J.B. Tender and Stephanie Allen (Nottingham University).

FUNDING

J.W.P. acknowledges financial support from KOSEF through Center for Integrated Molecular Systems, NCRC, and the Brain Korea 21 program. H.G.N. acknowledges financial support by the Korea Science and Engineering Foundation (KOSEF); NCRC grant funded by the Korea government (MEST) (R15-2004-033-05002-0). Funding for open access charges: NCRC.

Conflict of interest statement. None declared.

REFERENCES

1. St Johnston,D. (2005) Moving messages: the intracellular localization of mRNAs. *Nat. Rev. Mol. Cell. Biol*, **6**, 363–375.
2. Lécuyer,E., Yoshida,H., Parthasarathy,N., Alm,C., Babak,T., Cerovina,T., Hughes,T. R., Tomancak,P. and Krause,H. M. (2007) Global analysis of mRNA localization reveals a prominent role in organizing cellular architecture and function. *Cell*, **131**, 174–187.
3. Binnig,G., Quate,C.F. and Gerber,C. (1986) Atomic force microscope. *Phy. Rev. Lett.*, **56**, 930–933.
4. Müller,D.J. and Dufrêne,Y.F. (2008) Atomic force microscopy as a multifunctional molecular toolbox in nanobiotechnology. *Nat. Nanotechnol.*, **3**, 261–269.
5. Ros,R., Schwesinger,F., Anselmetti,D., Kubon,M., Schäfer,R., Plückthun,A. and Tiefenauer,L. (1998) Antigen binding forces of individually addressed single-chain Fv antibody molecules. *Proc. Natl Acad. Sci. USA*, **95**, 7402–7405.

6. Raab,A., Han,W., Badt,D., Smith-Gill,S.J., Lindsay,S.M., Schindler,H. and Hinterdorfer,P. (1999) Antibody recognition imaging by force microscopy. *Nat. Biotechnol.*, **17**, 901–905.
7. Kienberger,F., Ebner,A., Gruber,H. J. and Hinterdorfer,P. (2006) Molecular recognition imaging and force spectroscopy of single biomolecules. *Acc. Chem. Res.*, **39**, 29–36.
8. Ratto,T.V., Langry,K.C., Rudd,R.E., Balhorn,R.L., Allen,M.J. and McElfresh,M.W. (2004) Force spectroscopy of the double-tethered concanavalin-A mannose bond. *Biophys. J.*, **86**, 2430–2437.
9. Dupres,V., Menozzi,F.D., Locht,C., Clare,B.H., Abbott,N.L., Cuenot,S., Bompard,C., Raze,D. and Dufrêne,Y.F. (2005) Nanoscale mapping and functional analysis of individual adhesins on living bacteria. *Nat. Meth.*, **2**, 515–520.
10. Benoit,M., Gabriel,D., Gerisch,G. and Gaub,H.E. (2000) Discrete interactions in cell adhesion measured by single-molecule force spectroscopy. *Nat. Cell. Biol.*, **2**, 313–317.
11. Chtcheglova,L. A., Waschke,J., Wildling,L., Drenckhahn,D. and Hinterdorfer,P. (2007) Nanoscale dynamic recognition imaging on vascular endothelial cells. *Biophys. J.*, **93**, L11–L13.
12. Jones,L., López-Bendito,G., Gruss,P., Stoykova,A. and Molnár,Z. (2002) Pax6 is required for the normal development of the forebrain axonal connections. *Development*, **129**, 5041–5052.
13. Warren,N., Caric,D., Pratt,T., Clausen,J.A., Asavaritikrai,P., Mason,J.O., Hill,R.E. and Price,D.J. (1999) The transcription factor, Pax6, is required for cell proliferation and differentiation in the developing cerebral cortex. *Cereb. Cortex*, **9**, 627–635.
14. Englund,C., Fink,A., Lau,C., Pham,D., Daza,R.A.M., Bulfone,A., Kowalczyk,T. and Hevner,R.F. (2005) Pax6, Tbr2, and Tbr1 are expressed sequentially by radial glia, intermediate progenitor cells, and postmitotic neurons in developing neocortex. *J. Neurosci.*, **25**, 247–251.
15. Hevner,R.F., Hodge,R.D., Daza,R.A.M. and Englund,C. (2006) Transcription factors in glutamatergic neurogenesis: conserved programs in neocortex, cerebellum, and adult hippocampus. *Neurosci. Res.*, **55**, 223–233.
16. Kawaguchi,A., Ogawa,M., Saito,K., Matsuzaki,F., Okano,H. and Miyata,T. (2004) Differential expression of Pax6 and Ngn2 between pair-generated cortical neurons. *J. Neurosci. Res.*, **78**, 784–795.
17. Chauhan,B.K., Reed,N.A., Yang,Y., Ĉermák,L., Reneker,L., Duncan,M.K. and Cvekl,A. (2002) A comparative cDNA microarray analysis reveals a spectrum of genes regulated by Pax6 in mouse lens. *Genes to Cells*, **7**, 1267–1283.
18. Kawano,H., Fukuda,T., Kubo,K., Horie,M., Uyemura,K., Takeuchi,K., Osumi,N., Eto,K. and Kawamurai,K. (1999) Pax-6 is required for thalamocortical pathway formation in fetal rats. *J. Comp. Neurol.*, **408**, 147–160.
19. Pinto,L. and Götz,M. (2007) Radial glial cell heterogeneity – The source of diverse progeny in the CNS. *Prog. Neurobiol.*, **83**, 2–23.
20. Engel,A. and Müller,D.J. (2000) Observing single biomolecules at work with the atomic force microscope. *Nat. Struct. Mol. Biol.*, **7**, 715–718.
21. Hinterdorfer,P. and Dufrêne,Y.F. (2006) Detection and localization of single molecular recognition events using atomic force microscopy. *Nat. Meth.*, **3**, 347–355.
22. Gilbert,Y., Deghorain,M., Wang,L., Xu,B., Pollheimer,P.D., Gruber,H.J., Errington,J., Hallet,B., Haulot,X., Verbelen,C. *et al.* (2007) Single-molecule force spectroscopy and imaging of the vancomycin/D-Ala-D-Ala interaction. *Nano Lett.*, **7**, 796–801.
23. Dammer,U., Popescu,O., Wagner,P., Anselmetti,D., Guntherodt,H.-J. and Misevic,G.N. (1995) Binding strength between cell adhesion proteoglycans measured by atomic force microscopy. *Science*, **267**, 1173–1175.
24. Hugel,T. and Seitz,M. (2001) The study of molecular interactions by AFM force spectroscopy. *Macromol. Rapid Commun.*, **22**, 989–1016.
25. Zhang,W. and Zhang,X. (2003) Single molecule mechanochemistry of macromolecules. *Prog. Polym. Sci.*, **28**, 1271–1295.
26. Jung,Y.J., Hong,B.J., Zhang,W., Tendler,S.J.B., Williams,P.M., Allen,S. and Park,J.W. (2007) Dendron arrays for the force-based detection of DNA hybridization events. *J. Am. Chem. Soc.*, **129**, 9349–9355.
27. Lee,C.C., MacKay,J.A., Fréchet,J.M.J. and Szoka,F.C. (2005) Designing dendrimers for biological applications. *Nat. Biotechnol.*, **23**, 1517–1526.
28. Fréchet,J.M.J. and Tomalia,D.A. (2001) *Dendrimers and Other Dendritic Polymers*., Wiley, Chichester, New York.
29. Newkome,G.R., Moorefield,C.N. and Vögtle,F. (2001) *Dendrimers and Dendrons: Concepts, Syntheses, Applications*, Wiley–VCH, Weinheim, Germany.
30. Koo,B.-K., Lim,H.-S., Song,R., Yoon,M.-J., Yoon,K.-J., Moon,J.-S., Kim,Y.-W., Kwon,M., Yoo,K.-W., Kong,M.-P. *et al.* (2005) Mind bomb 1 is essential for generating functional Notch ligands to activate Notch. *Development*, **132**, 3459–3470.
31. Freier,S.M., Kierzek,R., Jaeger,J.A., Sugimoto,N., Caruthers,M.H., Neilson,T. and Turner,D.H. (1986) Improved free-energy parameters for predictions of RNA duplex stability. *Proc. Natl Acad. Sci. USA*, **83**, 9373–9377.